Straylight analysis for the externally occulted Lyot solar coronagraph ASPIICS

Raphaël Rougeot[a], Claude Aime[b], Cristian Baccani[e], Silvano Fineschi[f], Rémi Flamary[b], Damien Galano[a], Camille Galy[g], Volker Kirschner[a], Federico Landini[d], Marco Romoli[e], Sergey Shestov[c], Cédric Thizy[g], Jorg Versluys[a], and Andrei Zhukov[c]

[a]European Space Research and Technology Center, European Space Agency, Keplerlaan 1, 2201 Noordwijk, The Netherlands
[b]Laboratoire Lagrange, Université Côte d'Azur, Centre National de la Recherche Scientifique, Observatoire de la Côte d Ázur, Parc Valrose, 06108 Nice, France
[c]Solar-Terrestrial Centre of Excellence SIDC, Royal Observatory of Belgium, Avenue Circulaire 3, 1180 Brussels, Belgium
[d]Istituto Nazionale di Astrofisica, Arcetri Astrophysical Observatory, Largo E. Fermi 5, 50125 Firenze, Italy
[e]University of Florence, Dept.of Physics and Astronomy, Via Sansone 2, Sesto Fiorentino, Italy
[f]Istituto Nazionale di Astrofisica, Turin Astrophysical Observatory, Via Osservatorio 20, 10025 Pino Torinese, Italy
[g]Centre Spatial de Liège, Liège Science Park, 4031 Angleur (Liège), Belgium

ABSTRACT

The ESA formation Flying mission Proba-3 will fly the giant solar coronagraph ASPIICS. The instrument is composed of a 1.4 meter diameter external occulting disc mounted on the Occulter Spacecraft and a Lyot-style solar coronagraph of 50mm diameter aperture carried by the Coronagraph Spacecraft positioned 144 meters behind. The system will observe the inner corona of the Sun, as close as 1.1 solar radius. For a solar coronagraph, the most critical source of straylight is the residual diffracted sunlight, which drives the scientific performance of the observation. This is especially the case for ASPIICS because of its reduced field-of-view close to the solar limb. The light from the Sun is first diffracted by the edge of the external occulter, and then propagates and scatters inside the instrument. There is a crucial need to estimate both intensity and distribution of the diffraction on the focal plane. Because of the very large size of the coronagraph, one cannot rely on representative full scale test campaign. Moreover, usual optics software package are not designed to perform such diffraction computation, with the required accuracy. Therefore, dedicated approaches have been developed in the frame of ASPIICS. First, novel numerical models compute the diffraction profile on the entrance pupil plane and instrument detector plane (Landini et al., Rougeot et al.), assuming perfect optics in the sense of multi-reflection and scattering. Results are confronted to experimental measurements of diffraction. The paper reports the results of the different approaches.

Keywords: Diffraction, Sun, Coronagraphy, Formation Flying, Proba-3, ASPIICS

1. INTRODUCTION

The corona of the Sun is a hot, fully magnetized plasma, which governs the quiescence of the Sun and the space weather. Our knowledge about the heating mechanism in the corona, the dynamics of the coronal plasma, the acceleration process of the solar wind or the Coronal Mass ejections (CME), is still subject to active research. Among others, observation of the solar corona in white light is of first importance. However, its brightness is much fainter in this spectral band compared to the one of the solar disc itself. In fact, the K-coronal brightness ranges from 10^{-6} around $1.1R_\odot$ to 10^{-10} around $3R_\odot$ [1], with respect to the mean solar brightness, where $R_\odot$ is

Contact: raphael.rougeot@esa.int

the radius of the Sun. Therefore, almost perfect eclipse conditions are required, and high-contrast performance must be achieved to acquire relevant scientific data.
In the 1930s, Lyot proposed the novel concept of the coronagraph [2], which consists of focusing the light from the solar disc by a lens onto an occulting mask, and letting the faint coronal light propagating up to the detector. The development of coronagraphy has been continuously improving the straylight rejection performance. Evans [3] and Purcell and Koomen [4] investigated the use of an external occulter to block the sunlight before the entrance aperture of the imaging system. More advanced techniques for occultation were experimentally studied by Fort et al. [5] and Bout et al. [6]. The coronagraph LASCO C2 (Large Angle and Spectrometric Coronagraph) on the NASA mission SOHO [7] can be held as a successful example. We refer the interested reader to the review paper of Koutchmy [8] about the advent of spaceborne solar coronagraphy.
The coronagraph ASPIICS (Association de Satellites Pour l'Imagerie et l'Interférométrie de la Couronne Solaire) will fly on the ESA Formation Flying mission Proba-3 [9,10]. This novel mission concept will to virtually enlarge the instrument to unprecedented size. Both satellites will maintain a fixed Intersatellite Distance (ISD) of 144m, a millimeter accuracy, and will remain co-aligned with the Sun-pointing direction during the 6-hours apogee phase of a highly elliptical orbit 600km $\times$ 60500km. ASPIICS is composed of an external occulter of 1.4m diameter mounted on the Occulter Spacecraft (OSC), and a Lyot-style solar coronagraph carried by the Coronagraph Spacecraft (CSC). The refractive imaging system is based on the concept of Lyot, including an internal occulter and a Lyot stop aperture. ASPIICS will observe the corona in white light 540nm $-$ 570nm, with a plate scale resolution of 2.8arcsec. We refer the reader to the paper of Galano et al. [11] for a detailed description of the complete design of the instrument, and to the paper of Galy [12] for the optical design.
the major issue for coronagraphy, where high-contrast is required, is the straylight, and more particularly the diffraction of the bright light from the Sun. Because of the wave nature of light, diffraction effects occur from the edges of mechanical elements, especially occulters and apertures. Even if the occultation design is such that the light rays from the Sun are geometrically blocked, residual diffracted sunlight propagates and reaches the detector. This degradation of the quality of the observation is critical and thus must be assessed, in order to evaluate the scientific end-to-end performance of the instrument.
In the frame of the development of ASPIICS, several approaches have been conducted in parallel, in order to assess the diffraction straylight. First, a novel and dedicated analytical model has been developed in Matlab, based on Fresnel theory and Fourier optics formalism. This model analyses the diffraction wave propagation up to the detector plane. Second, numerical simulations were performed using the optical software package VirtualLab by Lightrans, to compute the umbra/penumbra level casted by the external occulter. In particular, this method allows analyze the optimized shape of ASPIICS external occulter. Finally, an experimental approach on an optical test-bench, using linear edges, was conducted. The present paper summarizes these different approaches and reports the results.
The paper is organized as follows. The first section contains this introduction. In the second section, we give a qualitative brief description of the straylight rejection design for ASPIICS. The third section treats the study of the umbra/penumbra casted by the external occulter. The fourth section presents the wave propagation model inside the Lyot-style coronagraph and reports the main results. Conclusions are given in the forth section.

2. QUALITATIVE DESCRIPTION OF ASPIICS STRAYLIGHT REJECTION

As briefly introduced in the previous section, the main objective of a solar coronagraph is to prevent the bright light of the Sun from reaching the detector. The fundamental concept of the Lyot solar coronagraph [2], as designed in the 1930s, consists of focusing the solar image on an occulting disc, named the Lyot mask, located at the focal plane of the telescope. The entrance aperture remains however fully illuminated, and produces unwanted diffraction straylight. The second idea of Lyot was to set a reduced stop aperture, named Lyot stop, in the image plane of the entrance pupil, where the diffraction annular fringe is focused.
The coronagraph ASPIICS improves that latter concept. The straylight rejection design uses first an external occulter, to cast an umbra cone on the entrance aperture of the instrument. This 710mm radius disc has a toroidal edge, whose radius of curvature is such that it mitigates the impact of potential tip/tilt. Nevertheless, diffraction effects occur because of the presence of the occulter which, in contradiction with pure geometrical predictions, makes the umbra be not perfectly dark. A preliminary interpretation is that, as viewed from the

instrument, the edge of the occulting disc seems to act as a virtual straylight source.
As such, it is expected that this diffracted light is imaged by the coronograph telescope optics as a bright circle which coincides with the geometrical image of the external occulter edge. The telescope focusses it on the conjugated plane of the external occulter, as defined by the laws of geometrical optics. This particular plane is located further then the focal plane of the telescope, because the disc is set at a finite distance. At this conjugated plane, a second occulting disc, named the internal occulter is located which serves as a mask to block the diffraction annular fringe. This reasonning has been confirmed by our dedicated diffraction modelling [13]. Finally, ASPIICS comprises also a Lyot stop to surpress additional diffraction effects from the pupil as described above.
The straylight performance of the complete system is thus driven by the rejection from the external occulter, i.e. how dark the umbra is, and the efficiency to cut diffraction of the internal occulter and the Lyot stop.

3. UMBRA FROM THE EXTERNAL OCCULTER

As explained above, the first part of the overall straylight analysis deals with the rejection by the external occulter. Here, we must estimate the umbra level, so the residual straylight power which enters the coronagraph. Three approaches were used concurrently in the frame of ASPIICS: an analytical model based on Fresnel diffraction theory, numerical simulations using the optical software VirtualLab by LightTrans, and a dedicated experimental study.

3.1 Fresnel diffraction

The Fresnel diffraction theory is based on wave optics, where the light is described by wave fronts following Fresnel free-space propagation [14]. The formulation requires paraxial approximation, i.e. small angles. Having an occulter of 1.4m located at 144m makes this assumption perfectly valid - the angles involved are $\simeq 10^{-2}$rad. This theory thus fits well our problem.
Our model is analytical, and follows the work of Aime [15]. The external occulter is assumed to be a perfect thin disc of radius $R = 710$mm, located at a distance $z_0 = 144.348$m from the entrance aperture plane, where z_0 corresponds to the ISD of Proba-3. Note that the value indicated in the text was used for the computation, but the ISD will actually have seasonal variations during the mission. The Sun is modeled as an extended incoherent light source of angular radius $R_\odot = 16.2$arcmin. We used monochromatic light at a wavelength $\lambda = 550$nm, and wavelength does not play a substantial role [16]. A solar limb darkening function is also implemented.
First, we computed the diffraction intensity pattern for the unitary on-axis point source at infinity, making use of Babinet's principle [14]. We denote by Ψ_0 the complex amplitude of the wavefront at the distance z_0 downstream to the external occulter. Taking advantage of the cylindrical symmetry of the geometry, Ψ_0 is written as a Hankel transformation:

$$\Psi_0(r) = 1 - \frac{e^{i\pi\frac{r^2}{\lambda z_0}}}{i\lambda z_0} \times \int_0^R 2\pi\rho \exp\left(i\pi\frac{\rho^2}{\lambda z_0}\right) J_0\left(2\pi\frac{r\rho}{\lambda z_0}\right) d\rho, \tag{1}$$

where r is the radial coordinate on the plane, counted from the center of the umbra, and $J_0(.)$ the Bessel function of the first kind. We performed an analytical computation, using the function NIntegrate of Mathematica [17]. The obtained diffraction intensity pattern $|\Psi_0(r)|^2$ is the famous bright spot of Arago, where the intensity is equal to 1 at the center of the umbra $r = 0$. This illustrates well the counter-intuitive nature of diffraction, being contradictory with the pure geometrical point of view.
To compute the penumbra profile at the distance z_0, we must integrate all the elementary diffraction intensity patterns from the solar point sources. Because of the small angular size of the Sun, we assumed that the diffraction pattern $|\Psi_0|^2$ is shift-invariant from one solar point source to another. It means that the intensity is shifted by a quantity $z_0 \times \tan\rho \simeq z_0 \times \rho$, where ρ is the angular high of the considered off-axis point source with respect to the center of the Sun.The penumbra is thus computed by performing a convolution of $|\Psi_0(x, y)|^2$ with the stenope image of the solar disc. Based on considerations of symmetry, the convolution can be reduced to a first integration along one solar radius, and then a circular integration. Denoting by $P(r)$ the radial penumbra intensity, we write

$$P(r) = \int_0^{2\pi} d\theta \int_0^{R_\odot} B(\rho)|\Psi_0(r + z_0 \times \rho, \theta)|^2 \rho d\rho, \tag{2}$$

where $B(\rho)$ is the radial centre-to-limb darkening function of the solar disc.
The computation was performed by a numerical integration in Matlab. The solar radius was sampled using 1000 points, which proved to be sufficient for the convergence of the integral.
Figure 1 plots the penumbra profile at z_0 $P(r)$ in black. The intensity is given in logarithmic scale, and normalized to 1 in full Sun, i.e. at $r = R + z_0 \times R_\odot = 1.381$m. The curve shows a dark inner region which extends up to $r = 38$mm: it defines the umbra cone. This radius perfectly matches to the geometrical size of the umbra given by $R - z_0 \times R_\odot$, plotted as a dotted vertical line in the plot. Here, the achieved umbra level is $10^{-3.9}$. Outside this central umbra region, the penumbra profile coincides to what a geometrical calculation would give, without any diffraction consideration, as shown in 13.
As a conclusion, this analysis showed that the external occulter, supposed with knife edge, already enables to decrease the solar irradiance by four order of magnitude at the entrance aperture of ASPIICS.

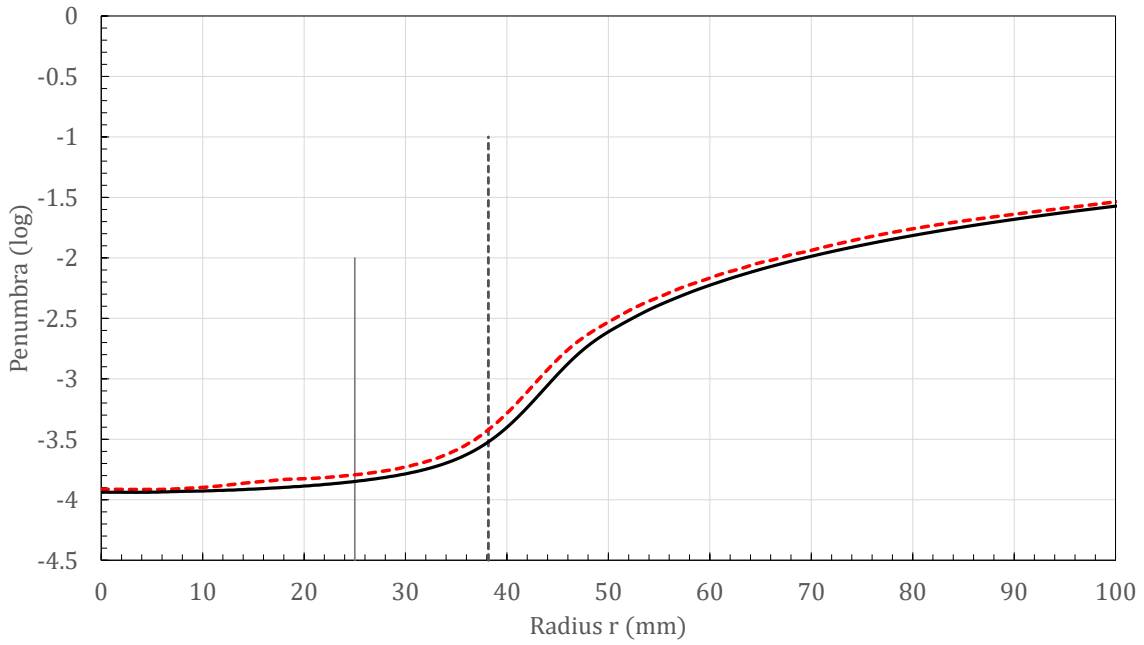

Figure 1. Penumbra profile $P(r)$ in logarithmic scale, function of the radius r in mm. The intensity is normalized to 1 in full sun. Black: analytical model from Fresnel diffraction theory, Sect.3.1. Red dashed: computation from VirtualLab, Sect.3.2. Plain vertical line: radius R_p of ASPIICS pupil. Dotted vertical line: umbra radius.

3.2 Computation using VirtualLab

An independent numerical approach was pursued by using the commercial optics design software VirtualLab Fusion [18].
A series of point sources evenly distributed over the solar disk were considered in order to simulate the photosphere. Each point source generates a plane wave that impinges on the external occulter with a certain inclination. The Spectrum of Plane Wave (SPW) operator included in the VirtualLab library was used to calculate the diffraction on the pupil plane as generated by the external occulter knife edge for each plane wave. Then, the patterns have been combined together. Using the same notation as previously, if $\Psi_\odot(x, y)$ is the impinging

plane wave, the propagation with the SPW operator can be written as:

$$\mathcal{P}_{z_0}^{SPW}\Psi_0 = \mathcal{F}^{-1}\left[\exp\left[i2\pi\sqrt{\frac{n^2}{\lambda^2}-\hat{x}^2-\hat{y}^2}\times z_0\right]\mathcal{F}\left[\Psi_\odot(x,y)\right]\right], \tag{3}$$

where $\lambda = 550$ nm is the wavelength, z_0 is the ISD, n =1 is the refractive index of the vacuum, $\hat{x}$ and $\hat{y}$ are the orthonormal coordinates in a spatial frequency frame of reference and $\mathcal{F}$ is the Fourier transform operator.
The result of the computation is plotted in dashed red in Fig.1, for a direct comparison to the Fresnel method. Despite both numerical approaches are rather different, the results coincide rather well in the umbra, which is governed by diffraction. The umbra level at the center is very similar - less than 5% of relative difference. Nevertheless, we note a discrepancy in the penumbra, starting from $r > 20$mm. The reason found is the following one.
In fact, the number of solar point sources drives the numerical accuracy and the computational time. We aimed to use VirtualLab simulation to compute the propagation of the fields through a much complex occulter design. Therefore, it was chosen to keep the number of point sources as low as possible in order to limit the required computation time while still having something physically and numerically comparable with the Fresnel diffraction formulation. We used a number of point sources that samples well the solar disk as far as the calculation in the umbra is concerned. It unfortunately leads to a slight overestimate of the penumbra. We verified that increasing the number of points actually decreases the observed discrepancy in the penumbra, at the price of a non-negligible increase of computational time.In conclusion, the implemented VirtualLab method proved to give reliable results in the umbra, which is the region of interest.
In case the diffraction behind a toroidal edge is concerned, a recent VirtualLab simulation performed according to the theory described in [19], whose results are subject of a forthcoming publication, showed that such toroidal occulter reduces the straylight in the umbra of about 68%, with respect to the knife-edged occulter.

3.3 Experimental approach from Landini et al.

An experimental approach is essential because some aspects may be left unaddressed by a purely theoretical study of diffraction. While a scaled model is under development, described in 20, the unique experimental data available are for the giant occulter demonstrator manufactured during phase A of ASPIICS project [19]. This experimental campaign demonstrated that a geometrical optimization of the occulter edge shape, even over a very short distance along the optical axis, improved the diffraction reduction performance of the occulter. It was the basis for the choice of a conical shape during the phase B and the definitive choice of a toroidal shape in phase C/D (mainly due to the need for respecting the strict manufacturing and alignment tolerances). The phase A external occulter demonstrator assumed that a small portion of the flight occulter could have been approximated by a linear edge. The diffraction was measured about 1m behind the occulter in the solid angle that would have been subtended by the flight pupil.
The accordance between data and simulation was great for the knife edge. The SPW operator of VirtualLab Fusion (described in Sect.3.2) has been used to simulate the diffraction behind one of the linear toroidal occulters of the phase A [21]. As shown in Fig.2, the toroidal shape of the linear edge is approximated by a series of 10 occulters, opportunely sized, over a finite distance of 20 mm, which corresponds to the length of the toroidal linear occulter used for the tests: each occulter is in the shadow of the previous one with respect to the solar disc light, and the toroidal surface is the envelope of the occulters edge. The diffraction propagation from a linear knife edge plane to the next was performed by means of the VirtualLab Fusion split-step beam propagation method described in [22]. The diffraction simulation behind the toroidal linear occulter has been the first ever for a linear occulter with an optimization shape along the optical axis.
The result of the simulation, compared with the data and the knife edge results, is shown in Fig.3. This analysis demonstrates that there actually is an improvement in the stray light reduction by properly modifying the occulter shape. Moreover, we now know that VirtualLab Fusion is experimentally validated as a flexible and reliable tool, provided that the sampling parameters are correctly set, to evaluate the diffraction behind both a knife and optimized edge.

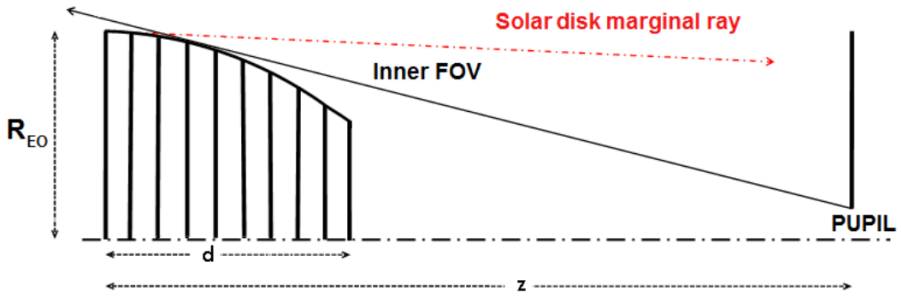

Figure 2. The toroidal linear edge was simulated by a series of linear knife edge occulters over a finite distance d, and he diffraction pattern was studied at a distance z.

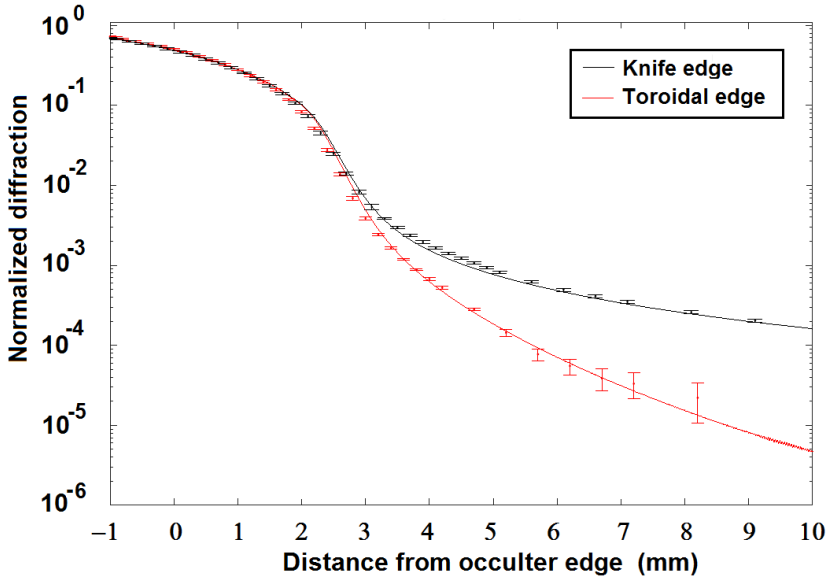

Figure 3. Comparison between the diffraction measured data for the linear knife edge and the linear toroidal edge. The simulated profiles are included as well as solid lines.

4. WAVE PROPAGATION INSIDE THE CORONAGRAPH

The second part of the straylight analysis aims to compute the propagation of the diffracted wave front through the the Lyot-style coronagraph up to the detector. A dedicated and novel numerical model has been developed accordingly, presented in Rougeot et al. [13].

4.1 Presentation of the model

The model is based on Fourier wave optics formalism, presented in [23], and follows the same approach as Aime et al. [24]. The coronagraph ASPIICS is represented by six remarkable successive planes along the optical z-axis:

- Plane O: the plane of the external occulter. The occulter is assumed a perfect thin disc located at $z_0 = 144.348$m upstream ASPIICS aperture, with a radius $R = 710$mm - like in Sect.3.1. As viewed from the center of the pupil, the inner field-of-view starts at $1.057 R_\odot$.

- Plane A: the plane of the entrance pupil. It is a circular aperture of radius $R_p = 25$mm. Here, we assume that the telescope L1 of focal length $f = 330.385$mm coincides with this plane.

- Plane B: focal plane of the telescope L1. In the original design of the Lyot coronagraph 2, so without external occulter, the image of the solar disc is focused in this plane, where the Lyot mask is set.

- Plane O': plane where is formed the image of the external occulter made by the telescope. It is the conjugate plane of plane O, at a distance $z_1 = f^2/(z_0 - f)$ from plane A. In ASPIICS, the internal occulter is set in this particular plane, instead of plane B. It is a perfect occulting disc of radius $R_{IO} = 1.642$mm, which gives to an over-occultation of $1.065 R_\odot$. The second objective L2 of focal f_2 also coincides with this plane.

- Plane C: the conjugate image plane of plane A, with respect to plane O'. The Lyot stop (a stop aperture) is located in this plane. Its radius is $R_L = 0.99 R_p$, which means 24.75mm with a 1:1 scale ratio between plane A and plane C. The third objective L3 of focal f_3 coincides with this plane - in the actual optical design, L3 is composed of a field of lenses.

- Plane D: final focal plane, where the detector is set.

Figure 4, adapted from [13], schematizes the model and the different planes.

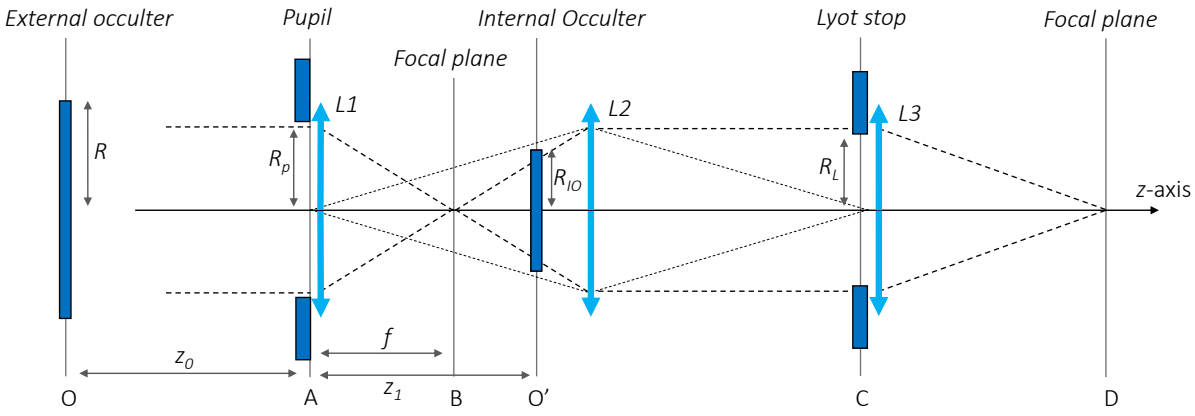

Figure 4. Schematic representation of ASPIICS, made of the successive planes O, A, B, O', C and D - adapted from [13]. The main parameters of the model are also reported. Figure not to scale.

The model relies on few assumptions. The entire instrument is assumed co-aligned with the Sun. No tilt nor lateral misalignment are yet considered - this will be introduced in the next section. In other words, the centers of the Sun, of the external occulter, of the entrance pupil, of the internal occulter and of the Lyot stop lie on the optical axis. All the defined planes are parallel with each others.
A second assumption is that the optics are perfect. No optical aberrations, nor surface roughness scattering is investigated at this stage. Forthcoming works from Rougeot et al. foresee the study of these effects.
The complete description and mathematical derivation of the method is given in the paper of Rougeot et al. [13]. Given one particular point source, the propagation of the wave front along the optical $z-$axis is computed sequentially, from one plane to the next one. It is described by a complex amplitude function in the transverse x, y-plane. We denote by $\Psi_{\mathcal{K}}(x, y; \alpha, \beta)$ this complex amplitude of the wave front in the particular plane $\mathcal{K} = A, B, O', C, D$ from the point source located at the angular coordinates α, β in the sky. We have:

$$\Psi_A\ (x, y; \alpha, \beta) = \exp\left(-2i\pi \frac{\alpha x + \beta y}{z_0}\right) \times \Psi_0(x + \alpha z_0, y + \beta z_0), \tag{4}$$

$$\Psi_B\ (x, y; \alpha, \beta) = \mathcal{F}_{\lambda f_1}\left[\Psi_A(\xi, \eta; \alpha, \beta) \times \mathcal{P}(\rho)\right], \tag{5}$$

$$\Psi_{O'}\ (x, y; \alpha, \beta) = \mathcal{F}_{\lambda z_1}\left[\Psi_A(\xi, \eta; \alpha, \beta) \times \mathcal{P}(\rho) \times \varphi_{-z_0}(\rho)\right], \tag{6}$$

$$\Psi_C\ (x, y; \alpha, \beta) = \mathcal{F}_{\lambda z_2}\left[\Psi_{O'}(\xi, \eta; \alpha, \beta) \times \mathcal{M}(\rho)\right] \times \varphi_{+z_0}(r), \tag{7}$$

$$\Psi_D\ (x, y; \alpha, \beta) = \mathcal{F}_{\lambda f_3}\left[\Psi_C(\xi, \eta; \alpha, \beta) \times \mathcal{L}(\rho)\right], \tag{8}$$

where $\mathcal{P}(\rho)$, $\mathcal{M}(\rho)$ and $\mathcal{L}(\rho)$ are respectively the radial functions representing the entrance pupil in plane A, the internal occulter in plane O' and the Lyot stop in plane C, where $\rho = \sqrt{\xi^2 + \eta^2}$ and $r = \sqrt{x^2 + y^2}$ are the transverse radii, $\varphi_z(r) = \exp(i\pi r^2/\lambda z)$ a quadratic phase term, and $\Psi_0(x, y) = \Psi_0(r = \sqrt{x^2 + y^2})$ is given by Eq.(1). Here, $\mathcal{F}_{\lambda z}$ is the two-dimension Fourier transformation with spatial frequency $u = x/\lambda z$ and $v = y/\lambda z$. Note that in the equations above (4) to (8), unnecessary propagation factors have been omitted.
The propagation described above was performed for one single point source. However, we are actually interested in the integrated intensity from the whole Sun. The solar disc is modeled by a collection of incoherent point sources. The axis-symmetry of the system makes the 2D image of one point source $|\Psi_{\mathcal{K}}(x, y; \alpha, \beta|^2$ rotate identically with its position on the solar disc. Consequently, instead of integrating over the full 2D solar disc, i.e. over α, β, we can integrate along one single solar radius, and then circularly integrate the obtained 2D image. If we denote by $I_{\mathcal{K}}(r)$ the radial integrated intensity in the particular plane $\mathcal{K}$, we have thus

$$I_{\mathcal{K}}(r) = \int_0^{2\pi} d\theta \int_0^{R_\odot} B(\alpha)|\Psi_{\mathcal{K}}(r, \theta; \alpha, 0)|^2 \alpha d\alpha, \tag{9}$$

where β has been arbitrary fixed to 0, and (r, θ) are the polar coordinates on plane $\mathcal{K}$, i.e. $x = r\cos\theta$ and $y = r\sin\theta$. Note the weight coefficient α to account for the polar surface element.

4.2 Numerical computation and analysis of the results

The computation of Eqs.(5) to (8) was performed using 2D-*FFT* routines in Matlab. On every plane, the wave front is sampled on large arrays of size $N \times N$. N was fixed to 2^{13} which proved to be accurate enough. The spatial sampling in plane A was carefully set according to a dedicated reasoning described in [13] (their Eq.(13)). The sampling on the other following planes is derived from *FFT* properties. The computation and related results presented in this paper was performed for the following set of parameters: $R_\odot = 16$arcmin, $z_0 = 144.348$m, $R = 710$mm, $R_p = 25$mm, $f = 330.385$mm, $R_{IO} = 1.642$mm and $R_L = 0.99R_p = 24.75$mm.
Figure 5 plots in red a radial cut of the diffraction intensity $I_{O'}(r)$ in the plane O', in logarithmic scale. As reference, the black curve shows the raw image of the solar disc. Here, the diffraction is well focused as a bright 10^{-2}-level peak. In two dimension, it consists of a circular fringe, located at $r = 1.629$mm. This radius corresponds exactly to the geometrical image of the edge of the external occulter made by the telescope. Qualitatively, it confirms that diffraction phenomenon acts as if the external occulter emits light, as discussed in Sect.2. The integrated flux which lies at $r < R_{IO}$ is blocked by the internal occulter, and does not propagate further.
As first conclusion, we demonstrated here the importance of the internal occulter for external coronagraphs, as

the it further rejects a major part of the diffracted light by cutting the bright diffraction fringe. Increasing its size R_{IO} improves well the rejection, but also degrades the inner field of view of the coronagraph. Finally, for the effective rejection of the straylight, one should well co-align both external and and internal occulters. In the case of Proba-3, the co-alignment of the of the two spacecraft flying in formation is thus critical for the scientific performance of ASPIICS.

Figure 6 gives the radial intensity $I_C(r)$ in plane C, in function of the radius given in units of pupil image. Similarly, the diffracted light focuses where the image of the edge of the entrance pupil is located. As shown, the Lyot stop is effective when its radius R_L is smaller than 1, in pupil image units. Although reducing the Lyot stop provides a substantial gain in rejection, it also reduces the overall throughput and resolution of instrument.

Figure 7 plots the final residual diffraction intensity $I_D(r)$ in plane D, in logarithmic scale. The radial pattern appears as a wide and defocused peak, as plane D is conjugated to infinity, i.e. the Sun, and not to plane O, since it was the case for plane O'. In the studied configuration, the diffraction fringe is about 10^{-6}, so comparable to the coronal brightness close to the solar limb.

Further analysis were performed by Rougeot et al. [13] about the impact of sizing the internal occulter and the Lyot stop on the residual diffracted sunlight on the final focal plane. The results showed that enlarging the internal occulter tends to decrease only the diffraction peak, while reducing the Lyot stop diminishes the straylight level over the whole field of view. Finally, we recall that the above diffraction curves were computed for an ideal geometry, and considering perfect optics. Therefore, the performance remains a theoretical upper boundary. Scattering from surface roughness or any misalignments of the formation should degrade these straylight levels.

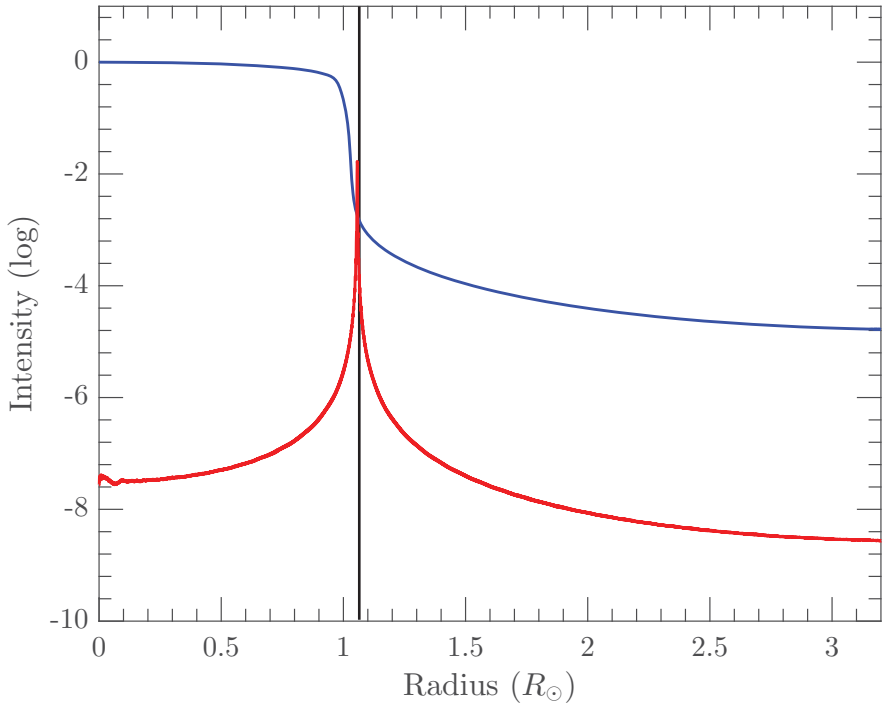

Figure 5. Radial intensity $I_{O'}(r)$ in plane O', normalized to mean solar brightness, in logarithmic scale. The radius r is reported in unit of equivalent angular solar radius $R_\odot$. Red: diffraction intensity, from the external occulter. Blue: raw image of the Sun, i.e. without external occulter, as reference. Vertical line: radius of the internal occulter. Figure adapted from [13].

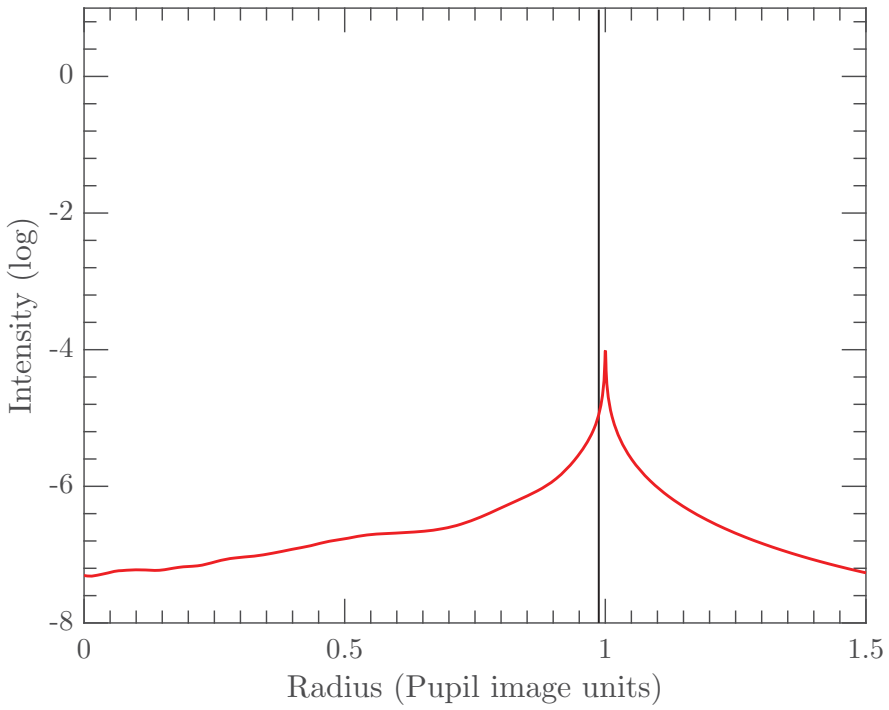

Figure 6. Radial intensity $I_C(r)$ in plane C, normalized to mean solar brightness, in logarithmic scale. The radius r is reported in unit of pupil image. Vertical line: radius of the Lyot stop. Figure adapted from [13].

4.3 Effects of misalignment and tilts

In a recent study, Shestov and Zhukov [16] built upon this model to include misalignments and tilts of the coronagraph. Only small angles were considered, of a tens of arcseconds, and lateral or longitudinal shifts of a few millimeters, in adequacy to Proba-3 formation flying requirements. In particular, they explained that any misaligned configuration can be reduced to the superposition of just two cases: a tilt of the telescope and a de-centering of the Sun.

For the numerical implementation, the integration over the solar disc must be performed using two dimension sampling, and the circular integration in Eq.(9) is no more applicable, since the axis-symmetry is now broken. When considering a lateral misalignment of an element, the occulter or the pupil for instance, related numerical mask is simply modeled with a spatial shift with respect to the optical axis. When considering a tilt by an angle ϕ in a certain direction $\overrightarrow{u}$ in the x, y-plane, a phase term of the form $\exp(2i\pi/\lambda\phi\overrightarrow{u})$ is multiplied accordingly. The simulation used the following parameters: $f = 330.348$mm, $R_{IO} = 1.662$mm and $R_L = 24.25$mm.

Figure 8 shows a cut of the intensity $I_D(x, y)$ of the residual diffracted sunlight in plane D for few misaligned or tilted configurations. The black dashed curve is the reference curve, where the coronagraphic system is perfectly co-aligned with the Sun. The blue curve accounts for an angular shift of 10arcsec of the Sun, with respect to the optical axis. The yellow curve accounts for the same tilt of 10arcsec of the telescope, the pupil remaining centered in the umbra cone. In both case, the straylight level increases, but not of the same amount. In fact, in the first case of a shift of the Sun, the angular apparent radius of the external occulter, i.e. $1.057R_\odot$, remains bigger than the angular solar radius $R_\odot$ incremented by 10arcsec. The external occultation is still effective. In the second case, the tilt of the telescope laterally shifts the location of the annular diffraction fringe in plane O'. Thus, the internal occulter is no more correctly positioned with respect to the diffraction pattern, so it does not block the straylight as it should. In other words, there is a leakage of diffracted light. This impact is much bigger. Finally, the red curve shows the diffraction intensity when the internal occulter is mispositioned along the optical axis, by a quantity $\delta z_1 = 60\mu$m. The impact on the straylight level remains small. Here, the diffraction

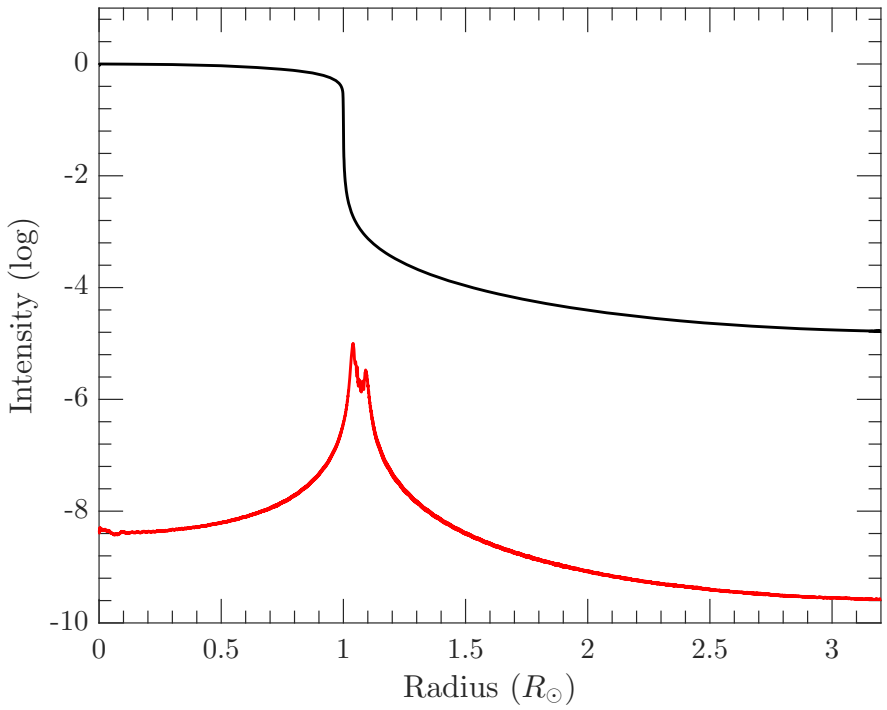

Figure 7. Radial intensity $I_D(r)$ in plane D, normalized to mean solar brightness, in logarithmic scale. The radius r is reported in unit of equivalent angular solar radius $R_\odot$. Red: diffraction intensity, from the external occulter. Black: raw image of the Sun, i.e. without any occulters, as reference. Figure adapted from [13].

fringe is no more focused in the plane of the internal occulter, and is thus more spread over this plane. The mask cut less flux, and the rejection performance is degraded.
We refer to the paper [16] for more study cases and further results.

5. CONCLUSION

In this paper, we presented and gave an overview of the different approaches to asses the straylight produced by the diffraction of the sunlight, in the frame of the externally occulted Lyot solar coronagraph ASPIICS. The thin external occulting disc produces an umbra with an intensity of $10^{-3.9}$ in the plane of the entrance apertrue [13,15,19]. A forthcoming publication, based on the implementation of [21] will present that the optimize toroidal shape reduces the straylight in the umbra of about 68%. The internal occulter and the Lyot stop rejects diffraction up to a level of 10^{-6} at $1.1R_\odot$ in the plane of the detector [13], so the same order of magnitude as the corona. The sensitivity of tilts and misalignments has been studied in [16].
As of now, there is no one particular method that enables, to itself only, analyzing the complete end-to-end straylight performance, considering the specificities of ASPIICS - large size, toroidal occulter, sensitivity and difficulty of experimental studies on diffraction. Then, applying, confronting and combining all the present methods remain necessary to address all the aspects of this problem.
At this stage of the project, the results of this overall straylight analysis is of crucial importance. First, as we showed, it supports the instrument design by driving the needed size of the internal occulter and the Lyot stop. Second, it enters in the definition of the scientific performance budget of ASPIICS. Finally, these models will support the post-processing of the science data.
Regarding the future activities, a scaled model to measure the diffraction pattern on the pupil plane has been

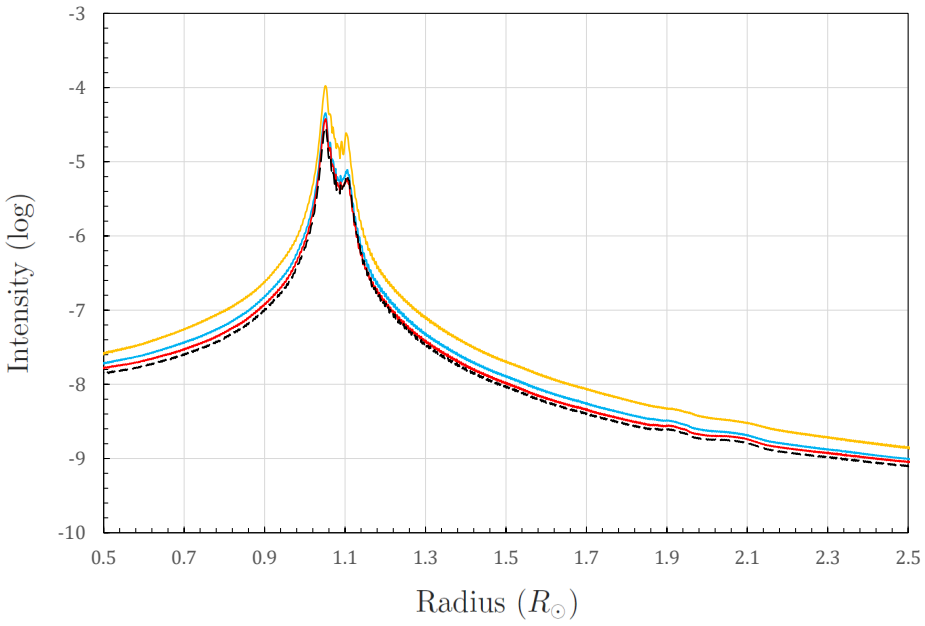

Figure 8. Radial cut of the intensity $I_D(x, y)$ in plane D, in logarithmic scale. The radius r is reported in unit of equivalent angular solar radius $R_\odot$. Dashed black: co-aligned system. Blue: angular shift of the Sun of 10 arcesc. Yellow: tilt of the telescope of 10arcsec. Red: longitudinal shift of the internal occulter (plane O') by a quantity $\delta z_1 = 60\mu$m.

designed and will be soon implemented as described in [20]. Moreover, a work combining experimental measurements and VirtualLab simulation on the toroidal occulter will be presented in a forthcoming paper. In parallel, the wave propagation model is currently improved in order to take into account optical aberration effects and scattering from surface roughness on the diffraction.

ACKNOWLEDGMENTS

We would like to thank the European Space Agency and the Proba-3 project for the fundings and the support of these activities.

REFERENCES

[1] Cox, A., [*Allens astrophysical quantities*], New York AIP Press, Springer (2000).
[2] Lyot, B., "The study of the solar corona and prominences without eclipses," *MNRAS* **99**, 580 (1939).
[3] Evans, J., "A photometer for measurement of sky brightness near the sun," *J. Opt. Soc. Am.* **88**, 1083 (1948).
[4] Purcell, J. and Koomen, M., "Coronaraph with improved scattered-light properties," *Report of NRL Progress, US GPO, Washington, D.C.* (1962).
[5] Fort, B., Morel, C., and Spaak, G., "Theoretical performance of solar coronagraphs using sharp-edged or apodized circular external occulters," *Astron. Astroph.* **63**, 243–246 (1978).
[6] Bout, M., Lamy, P., Maucherat, A., Colin, C., and Llebaria, A., "Experimental study of external occulters for the large angle and spectrometric coronagraph 2: Lasco-c2," *Applied Optics* **39, 22**, 3955–3962 (2000).

[7] Brueckner, G., Howard, R., Koomen, M., Korendyke, C., Michels, D., Moses, J., Socker, D., Dere, K., P.L. Lamy, A. L., Bout, M. V., Schwenn, R., Simnett, G., Bedford, D., and Eyles, C., "The large angle sprectroscopic coronagraph," *Solar Physics* **162**, 357–402 (1995).

[8] Koutchmy, S., "Space-borne coronagraphy," *Sci. Rev.* **47**, 95 (1988).

[9] Lamy, P., Damé, L., Vivès, S., and Zukhov, A., "Aspiics: a giant coronagraph for the esa/proba-3 formation flying mission," *Proc. SPIE* **7731**, 18 (2010).

[10] Renotte, E., "Recent achievements on aspiics, an externally occulted coronagraph for proba-3," (2016).

[11] Galano, D., Buckley, S., Cernica, I., Daniel, V., Denis, F., de Vos, L., Fineschi, S., Galy, C., Graczyk, R., Horodyska, P., Jacob, J., Jansen, R., Kranitis, N., Kurowski, M., Ladno, M., Ledent, P., Loreggia, D., Melich, R., Mollet, D., Mosdorf, M., Paschalis, A., Peresty, R., Radzik, B., Rataj, M., Rougeot, R., Salvador, L., Thizy, C., Versluys, J., Walczak, T., Zarzycka, A., Zender, J., and Zhukov, A., "Development of aspiics: a coronagraph based on proba-3 formation flying mission," *Proc. SPIE* **10698**, 10698–104 (2018).

[12] Galy, C., Fineschi, S., Galano, D., Howard, R., Kintziger, C., Kirschner, V., Koutchmy, S., Lamy, P., Mazzoli, A., Melich, R., Mestreau-Garreau, A., Renotte, E., Servaye, J., Stockman, Y., Thizy, C., and Zhukov, A., "Design and modelisation of aspiics optics," *Proc. SPIE* **9604**, 96040 (2015).

[13] Rougeot, R., Flamary, R., Galano, D., and Aime, C., "Performance of the hybrid externally occulted lyot solar cornagraph," *A&A* **599**, A2 (2017).

[14] Born, M. and Wolf, E., [*Principles of optics*], Cambridge University Press (2011 (seventh edition)).

[15] Aime, C., "Theoretical performance of solar coronagraphs using sharp-edged or apodized circular external occulters," *A&A* **558**, A138 (2013).

[16] Shestov, S. and Zhukov, A., "Influence of misalignments on performance of externally occulted solar coronagraphs," *A& A* **612**, A82 (2018).

[17] "Wolfram 2012, mathematica (champaign, il: Wolfram research, inc.)."

[18] Lighttrans (25 January 2017). http://www.lighttrans.com.

[19] Landini, F., Vives, S., Vent, M., Romoli, M., and guillon S. Fineschi, C., "External occulter laboratory demonstrator for the forthcoming formation flying coronagraphs," *Applied Optics* **50(36)**, 6632 (2011).

[20] Landini, F., Baccani, C., Vives, S., Fineschi, S., Romoli, M., Capobianco, G., Massone, G., Casti, M., Bemporad, A., Focardi, M., Pancrazzi, M., Loreggia, D., Noce, V., Corso, A. J., Thizy, C., Renotte, E., and Marquet, B., "Test plan for the proba3/aspiics scaled model measurement campaign," *Proc. SPIE* **10397**, 103971C–1 (2017).

[21] Baccani, C., Landini, F., Romoli, M., Taccola, M., Schweitzer, H., Fineschi, S., Bemporad, A., Loreggia, D., Capobianco, G., Pancrazzi, M., Focardi, M., Noce, V., Thizy, C., Servaye, J., and Renotte, E., "Preliminary evaluation of the diffraction behind the proba 3/aspiics optimized occulter," *Proc. SPIE* **9904**, 990450–1 (2016).

[22] Landini, F., Romoli, M., Baccani, C., Focardi, M., Pancrazzi, M., Galano, D., and Kirschner, V., "Scaled model guidelines for solar coronagraphs external occulters with an optimized shape," *Optics Letters* **42 (23)**, 4800 (2017).

[23] Goodman, J., [*Introduction to Fourier optics*], Roberts and Company Publishers (2005).

[24] Aime, C., Soummer, R., and Ferrari, A., "Total coronagraphic extinction of rectangular apertures using linear prolate apodizations," *A&A* **389**, 334 (2002).